IEEE Access
Multidisciplinary | Rapid Review | Open Access Journal

SPECIAL SECTION ON ADVANCES IN PROGNOSTICS AND SYSTEM HEALTH MANAGEMENT

Received May 31, 2019, accepted June 18, 2019, date of publication June 26, 2019, date of current version July 17, 2019.

Digital Object Identifier 10.1109/ACCESS.2019.2924832

Fault Diagnosis Accuracy Improvement Using Wayside Rectangular Microphone Array for Health Monitoring of Railway-Vehicle Wheel Bearing

HAIDONG HUANG[1], FANG LIU[1,2], LIN GENG[1], YONGBIN LIU[1,2], ZIHUI REN[3,5], YUKUN ZHAO[3,5], XIUJUN LEI[4,5], AND XIAOYIN LU[4,5]

[1]College of Electrical Engineering and Automation, Anhui University, Hefei 230601, China
[2]National Engineering Laboratory of Energy-Saving Motor and Control Technology, Anhui University, Hefei 230601, China
[3]Anhui Fuhuang Technology Company Ltd., Hefei 230088, China
[4]Hefei Fuhuang Junda High-Tech Information Technology Company Ltd., Hefei 230031, China
[5]Anhui Fuhuang Steel Structure Company Ltd., Hefei 238076, China

Corresponding author: Fang Liu (ufun@foxmail.com)

This work was supported in part by the National Natural Science Foundation of China under Grant 51875001, Grant 51675001, and Grant 51705001, in part by the Key Research and Development Plan of Anhui Province under Grant 201904A05020034, and in part by the Major Science and Technology Project in Anhui Province under Grant 17030901047.

ABSTRACT Wayside acoustic detection is a promising technology for railway-vehicle bearing health monitoring due to its merits of non-conduct measurement, low cost, and early warning capacity. However, the diagnostic accuracy will be reduced by the problems of strong background noise and Doppler distortion. Considering the super spatial directivity ability of the microphone array, in this paper, a uniform rectangular array (URA) and an optimal spatial filter (OSF) based on the principle of minimum variance distortion-less response (MVDR) are designed to improve the diagnostic accuracy. Compared with the traditional single microphone and linear array, spatial directivity can be improved significantly so that the better anti-noise performance and higher diagnostic accuracy can be achieved. First, a URA consisting of 15 microphone elements arranged into five columns and three rows is designed to capture the wayside acoustic signal. Second, the direction angle of the target moving sound source with high accuracy is calculated at different times. Third, an OSF based on the principle of the MVDR is designed to extract the target sound source signal. Fourth, Doppler effect embedded in the filtered signal is eliminated using the MVDR spectrum estimation and resampling method. Finally, the diagnosis decision is made through an envelope spectrum analysis. The comparative simulation and experimental case studies are carried out to verify the effectiveness and improvement of the proposed method.

INDEX TERMS Acoustic defective bearing detection, Doppler effect, fault diagnosis, microphone array, MVDR.

I. INTRODUCTION

Railway transportation plays an important role in nowadays transportation. Ensuring the safe operation of railway vehicles has become an important mission of railway transportation under the situation of rapid railway speed increase in recent years. Wheel bearing is a key part of railway vehicles [1]–[5]. Traffic accidents caused by railway-vehicle bearing failure will bring huge losses and even disasters [6]–[10]. Therefore, it is of great significance for condition monitoring of the railway-vehicle bearings. Nowadays, many non-disassembling diagnosis techniques have emerged such as oil monitoring [11], hot-box detection [12]and acoustic emission [13], [14]. Especially, vibration analysis such as stochastic resonance [15]–[17], support vector machines [18], [19], morphological analysis [20], local mean decomposition [21], wavelet packet transform [22], [23] and wavelet transform (WT) [24]–[26]. Wayside acoustic

The associate editor coordinating the review of this manuscript and approving it for publication was Dong Wang.

defective bearing detector (ADBD) is a technique developed in recent years [27]–[29]. In the ADBD system, microphones are arranged on both sides of the tracks. Acoustic signals emitting from the railway-vehicle bearings are collected when vehicle pass-by and the health condition of the bearings is decided through analysis of the collected signal. Compared with other methods, it has advantages of non-contact [30], low costs and early failure detection ability [31].

However, there are two important issues that make it difficult to diagnose accurately including strong background noise and Doppler distortion. In the current research, one microphone or the uniform linear array (ULA) is used to capture the wayside bearing acoustic signal. And the aforementioned two problems are generally solved in the stage of signal processing [32]–[35]. For instance, a kind of Doppler-let filter is constructed to remove noise effectively by Zhang *et al* [36]. This method requires the velocity of the vehicle in advance and it is difficult to determine the thresholds in the time frequency filter. Wang *et al* proposed a method combining continuous wavelet transform with manifold learning. In this method, the multi-scale manifold ridge line is extracted from the time-scale plane to realize the demodulation of the fault signal of the bearing [37]. It can eliminate both scale noise and in-band noise at the same time, but the computational complexity is high. Zhang *et al* achieved the separation by seeking the time-varying statistical characteristics of different components of the signal in the singular value space according to the Time-varying Singular Value Decomposition (TSVD) [38]. It has the advantages of eliminating in-band noise, preserving harmonic components and improving the accuracy of spectrum identification of transient components. However, there are some problems such as incomplete theoretical basis, tendency term of singular value sequence and the high cost of calculation.

On the other hand, many methods have been studied on the problem of Doppler distortion. Liu et al. proposed a time-domain interpolation resampling (TIR) based on kinematic model [39]. It does not need to know the characteristic frequency beforehand, but it depends on the moving parameters most of which are unknown in practice. To solve this problem, the resampling methods based on instantaneous frequency estimation (IFE) are studied by researchers, such as Hilbert transform (HT) [31] and the short-time Fourier transform (STFT) [40]. The resampling time series can be obtained by IFE from the wayside signal, so it has the advantage of realizing automatic correction without external sensors. However, when the background noise is strong, the extraction of instantaneous frequency becomes difficult. Liu et al. further proposed a method based on matching pursuit to estimate the parameters by Doppler-let transform [41]. Although it performs well, huge computation requirement makes it difficult to realize real-time diagnosis.

It should be noted that only one single microphone is used in the above methods and the emphasis is put on the stage of signal processing. Recently, a uniform linear array (ULA) and a time-varying spatial filtering rearrangement (TSFR) scheme are firstly introduced by Zhang *et al.* [42]. Comparing those methods with one single microphone, more microphones are employed to capture the signal simultaneously and the spatial filter based on the mechanism of time delay of the multipath signals can be designed for signal-to-noise (SNR) enhancement and adaptive Doppler Effect elimination. In Zhang's method, the spatial filter is constructed depending on the source location and has little relationship with the signal energy, so this method has significant advantages in when the background noise is heavy in comparison with methods using one single microphone. However, the ULA has poor vertical spatial directivity because the microphones are only arranged along the horizontal direction. As a result, there is an error in the estimated sound source location and the jump phenomenon emerges when the sound source is relatively far from the microphone. Later, Liu *et al* proposed a matching pursuit algorithm combined with ULA [43]. The adaptive correction of Doppler distortion can be achieved by identifying and obtained parameters through parameterized atomic matching. However, Because of the large number of atomic parameters, the amount of calculation is relatively large.

In this study, a URA is firstly introduced as the wayside signal acquire device and an optimal spatial filter (OSF) based on the principle of Minimum Variance Distortion-less Response (MVDR) [44]–[46] is designed to extract the target sound source signal. Compared with the traditional ULA, it has the following merits:

1) Due to the additional microphone arrangement in the vertical direction, the elevation angle can be acquired and so that the spatial resolution of the array can be improved significantly. As a result, better anti-noise performance can be achieved.
2) Because the spatial location of the acoustic source can be estimated much more accurately, the time series for resampling can be calculated more accurately, so that Doppler Effect can be better eliminated.
3) In this study, the OSF is constructed based on the principle of MVDR, so it has little relationship with the signal energy. It has significant advantages in comparison with traditional methods using one single microphone or ULA.

Comparative simulation and experimental case studies in this study have shown the improvement of anti-noise performance and diagnostic accuracy. The rest of this paper is organized as follows. In section 2, the proposed method is introduced in detail including the design of the URA, the OSF and the Doppler distortion correction scheme. Simulation and three experimental case studies are given in Section 3 and 4 respectively. Finally, conclusions are given in section 5.

II. METHOD

A. WAYSIDE URA MODEL

The basic model containing a moving acoustic source (bearing) passing by a ULA and a URA are shown in

TABLE 1. Variables.

Symbol	Quantity	Symbol	Quantity
t_c	central moment	θ	azimuth angle
φ	elevation angle	t_s	the emitting time,
t_r	the received time	M_c	Mach
dt	the delay time	c	sound velocity
$\boldsymbol{A}(\theta)$	the director vector matrix	x	the received signal
s_{obj}	the object source	$\mathbf{N}$	the addition noise
P	the sound pressure	E	the mathematical expectation
$\boldsymbol{R}_{xx}$	the covariance matrix	$\boldsymbol{w}_{obj}$	the optimal weight
$R_{(m1m2)}$	the distance between the sound source and the microphone		

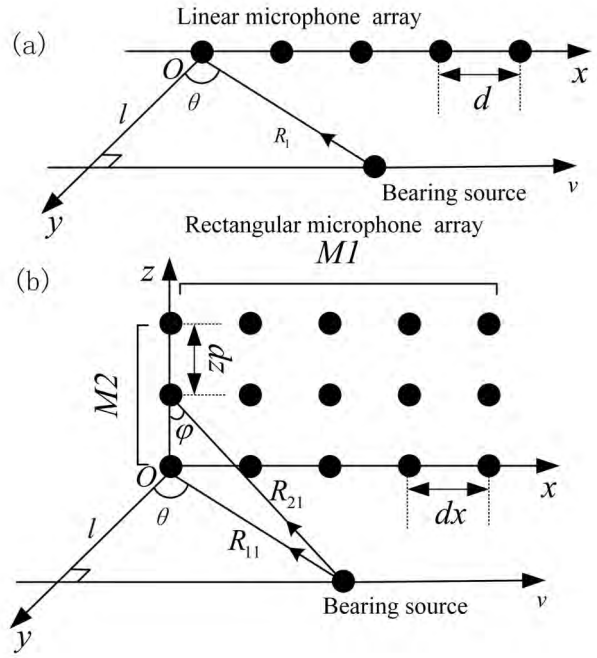

FIGURE 1. Basic model of (a) ULA and (b) URA.

Fig. 1(a) and (b) respectively. The acoustic source moves along the direction of the x-axis with a uniform speed. It can be seen that compared with ULA, the elevation angle can be distinguished through URA and so that the spatial resolution of the array can be improved.

In this study, the URA consisted of microphone elements arranged into M_1 rows and M_2 columns on a specific panel is placed perpendicular to the direction of source moving and l is the distance between the plane of the array and the line along which the sound source moves in Fig.1. The bottom of the array is on the same horizontal plane with the sound source. The horizontal distance between adjacent microphones is dx, and the vertical distance is dz. θ denotes the azimuth and φ represents the elevation of source. $R_{(m1m2)}(m_1 = 1, 2, \ldots M_1; m_2 = 1, 2, \ldots M_2)$ denotes the distance between the sound source and the microphone.

During the sound source moving passing by the array, there is a time $t_c(m_1, m_2)$ when the acoustic source moves nearest to the microphone element located at (m_1, m_2) which can be expressed as:

$$t_c(m_1, m_2) = t_c(m_1, 1) = t_c(1, 1) + (m_1 - 1) \times dx/v \quad (1)$$

where v denotes the moving speed. According to the geometrical relationship as shown in Fig.1 (b), the distance between the sound source and the microphone located at (m_1, m_2) can be calculated using the following equation:

$$R_{(m_1m_2)}(t_s) = \sqrt{l^2 + (vt_c(m_1, m_2) - vt_s)^2 + [(m_2 - 1)dz]^2} \quad (2)$$

where ts denotes the sound emitting time of the acoustic source. The time when the microphone received the sound can be calculated using the following equation:

$$t_r = t_s + dt \quad (3)$$

where dt denotes the time delay between the emitting time and the receiving time which can be calculated as:

$$dt = R_{(m_1m_2)}(t_s)/c \quad (4)$$

where c denotes the speed of sound propagation in the air and can be regarded a constant of 340 m/s in the air.

Assume that the bearing acoustic source is a monopole point and the propagation medium is an ideal fluid without energy loss. According to Morse's theory Morse's theory of acoustics [47], based on the wave equations and motion relationship, the sound pressure $P(t_r)$ at time t_r can be expressed as follows:

$$P(t_r) = \frac{q'(t_r - R_{m_1m_2}(t_s)/c)}{4\pi R_{m_1m_2}(t_s)[1 + M_c \sin\theta(t_s)]^2} + \frac{q'(t_r - R_{m_1m_2}(t_s)/c)v[\sin\theta(t_s) - M_c]}{4\pi R^2_{m_1m_2}(t_s)[1 + M_c \sin\theta(t_s)]^3} \quad (5)$$

where $M_c = v/c$, and the $\sin\theta(t_s)$ can be expressed as:

$$\sin\theta(t_s) = \frac{vt_s - vt_c(m_1, m_2)}{\sqrt{l^2 + [vt_c(m_1, m_2) - vt_s]^2}} \quad (6)$$

q is the total flow rate of monopole point sound source mass and M_c is the Mach number. The first term of Eq. (5) represents the sound field radiation term attenuated by propagation distance, and the second term is the near-field effect. When the far-field measurement condition is satisfied or the moving Mach number of sound source is lower than 0.2, compared with the first term, the second term is small and can be ignored. Therefore, the sound pressure received is approximately:

$$x_{m_1m_2}(t_r) = \frac{q'(t_r - R_{m_1m_2}(t_s)/c)}{4\pi R_{m_1m_2}(t_s)[1 + M_c \sin\theta(t_s)]^2} \quad (7)$$

and the array signals can be written in a discrete form as follows:

$$\boldsymbol{X} = [\boldsymbol{x}_{11}, \boldsymbol{x}_{12}, \cdots, \boldsymbol{x}_{21}, \cdots, \boldsymbol{x}_{M_1M_2}] \quad (8)$$

where $\boldsymbol{x}_{m1m2} = [x_{m1m2}(t_r(1)), x_{m1m2}(t_r(2)), \ldots, x_{m1m2}(t_r(N))]$, and N denotes the length of signal.

B. SIGNAL MODEL OF URA

In this study, the URA is designed to satisfy far-field model condition [48], [49]:

$$l > \frac{2[dx(M_1 - 1)]^2}{\lambda} \tag{9}$$

where λ denotes the wavelength of the sound source. Under this condition, the sound wave collected by the array can be seen as plane waves.

According to Eq. (6), the acoustic source is moving and it can be regarded as a point source at each sound emitting time. Assuming that there are a number of Q far-field narrowband signal incidents on the array, according to Fig.1(b), taking the array element at the origin as a reference point, the time delay between the i-th signal received by the m-th array element and the i-th signal received by the reference array element can be expressed as:

$$\tau_{m_1 m_2} = \frac{1}{c}[(m_1 - 1)dx \sin\theta \sin\varphi + (m_2 - 1)dz \cos\varphi] \tag{10}$$

The matrix form of the received signal can be expressed as:

$$\boldsymbol{X}(\boldsymbol{t}) = \boldsymbol{A}(\theta(\boldsymbol{t}), \varphi(\boldsymbol{t}))\boldsymbol{S}(\boldsymbol{t}) + \boldsymbol{N}(\boldsymbol{t}) \tag{11}$$

where $\boldsymbol{A}(\theta, \varphi) \in R^{M1\ M2 \times Q}$ is a direction vector matrix, which can be written as follows:

$$\begin{aligned} A(\theta(t), \varphi(t)) = [&a(\theta_{obj}(t), \varphi_{obj}(t)), a(\theta_1(t), \varphi_1(t)), \\ &\cdots, a(\theta_{Q-1}(t), \varphi_{Q-1}(t))]_{M_1 M_2 \times Q} \end{aligned} \tag{12}$$

where the direction vector $\boldsymbol{a}(\theta_k(t), \varphi_k(t))$ ($k = obj, 1, 2, \ldots,$ Q-1) can be written as follows.

$$\begin{aligned} &\boldsymbol{a}(\theta_k(t), \varphi_k(t)) \\ &\quad = [e^{-j\omega\tau_{11}}, e^{-j\omega\tau_{12}}, \cdots, e^{-j\omega\tau_{m_1 m_2}}, \cdots, e^{-j\omega\tau_{M_1 M_2}}] \end{aligned} \tag{13}$$

$$\omega = \frac{2\pi}{T} = 2\pi f_c \tag{14}$$

where f_c denotes the natural frequency of the signal.

$$\boldsymbol{S}(\boldsymbol{t}) = [\boldsymbol{s}_{obj}(\boldsymbol{t}), \boldsymbol{s}_1(\boldsymbol{t}), \boldsymbol{s}_2(\boldsymbol{t}), \cdots, \boldsymbol{s}_q(\boldsymbol{t}), \cdots, \boldsymbol{s}_{Q-1}(\boldsymbol{t})]^T \tag{15}$$

where $\boldsymbol{s}_{obj} \in R^{1\times N}$ denotes the object source with the length of N, $\boldsymbol{s}_q \in R^{1\times N}$ ($q = 1, 2, \ldots, Q$-1) denotes the Q -1 interference sources, $\boldsymbol{N}(t) \in R^{1\times N}$ denotes the additive noise.

Therefore, the signals received by the $M_1 \times M_2$ array elements at the time tr can be arranged into a column vector, which can be expressed as:

$$\begin{bmatrix} \boldsymbol{x}_{11}(\boldsymbol{t}) \\ \boldsymbol{x}_{12}(\boldsymbol{t}) \\ \vdots \\ \boldsymbol{x}_{M_1 M_2}(\boldsymbol{t}) \end{bmatrix} = \begin{bmatrix} \boldsymbol{e}^{-jw\pi_{(11,1)}} & \boldsymbol{e}^{-jw\pi_{(11,2)}} & \cdots & \boldsymbol{e}^{-jw\pi_{(11,Q)}} \\ \boldsymbol{e}^{-jw\pi_{(12,1)}} & \boldsymbol{e}^{-jw\pi_{(12,2)}} & \cdots & \boldsymbol{e}^{-jw\pi_{(12,Q)}} \\ \vdots & \vdots & \ddots & \vdots \\ \boldsymbol{e}^{-jw\pi_{(M_1M_2,1)}} & \boldsymbol{e}^{-jw\pi_{(M_1M_2,2)}} & \cdots & \boldsymbol{e}^{-jw\pi_{(M_1M_2,Q)}} \end{bmatrix} \times \begin{bmatrix} \boldsymbol{s}_1(\boldsymbol{t}) \\ \boldsymbol{s}_2(\boldsymbol{t}) \\ \vdots \\ \boldsymbol{s}_Q(\boldsymbol{t}) \end{bmatrix} + \begin{bmatrix} \boldsymbol{n}_{11}(\boldsymbol{t}) \\ \boldsymbol{n}_{12}(\boldsymbol{t}) \\ \vdots \\ \boldsymbol{n}_{M_1 M_2}(\boldsymbol{t}) \end{bmatrix} \tag{16}$$

Eq. (16) is the matrix form of Eq. (11).

C. OSF BASED ON THE PRINCIPLE OF MVDR

With the signal model given in Eq. (11), the signal passes through a set filter $\boldsymbol{w}$ and the filter weight can be expressed as:

$$\boldsymbol{w} = [w_{11}, w_{12}, \cdots w_{1M_2}, w_{21}, \cdots, w_{m_1 m_2} \cdots, w_{M_1 M_2}]^T \tag{17}$$

where superscript T denotes transposition. The filtered signal y can be obtained by the following equation:

$$\boldsymbol{y} = \boldsymbol{w}^H \boldsymbol{X} \tag{18}$$

And its power is:

$$E\left\{\left|y_{m_1 m_2}(n)\right|^2\right\} = E\left\{\left|w^H_{m_1 m_2} x(n)\right|^2\right\} = w^H_{m_1 m_2} \boldsymbol{R}_{xx} w_{m_1 m_2} \tag{19}$$

where E is the mathematical expectation, superscript H denotes transpose conjugate of a vector or a matrix. $\boldsymbol{R}_{xx}$ is the covariance matrix of the input signal $\boldsymbol{x}(n)$ which can be calculated as:

$$\boldsymbol{R}_{xx} = E\left\{x(n)x^H(n)\right\} \tag{20}$$

The filter w_{m1m2} is designed to minimize its output power subject to the constraint that its response at the interest f_c has unity gain. This constraint, knows as the distortion-less constraint, can be written as:

$$\boldsymbol{w}^H \boldsymbol{a}(\theta_{obj}(t), \varphi_{obj}(t)) = 1 \tag{21}$$

Mathematically, the distortion-less filter w_{m1m2} is obtained by solving the following constrained optimization problem:

$$\begin{aligned} \boldsymbol{w}_{obj} = &\min_{\boldsymbol{w}} \ \boldsymbol{w}^H \mathbf{R}_{xx} \boldsymbol{w} \\ &\text{subject to } \boldsymbol{w}^H \boldsymbol{a}(\theta_{obj}(t), \varphi_{obj}(t)) = 1 \end{aligned} \tag{22}$$

The solution to this constrained optimization problem is

$$\boldsymbol{w}_{obj} = \frac{\boldsymbol{R}_{xx}^{-1} \boldsymbol{a}(\theta_{obj}(t), \varphi_{obj}(t))}{\boldsymbol{a}^H(\theta_{obj}(t), \varphi_{obj}(t)) \boldsymbol{R}_{xx}^{-1} \boldsymbol{a}(\theta_{obj}(t), \varphi_{obj}(t))} \tag{23}$$

The azimuth spectrum estimate of the target can be expressed by the following equation:

$$\boldsymbol{P}_{MVDR} = \frac{1}{\boldsymbol{a}^H(\theta(\boldsymbol{t}), \varphi(\boldsymbol{t})) \boldsymbol{R}_{xx}^{-1} \boldsymbol{a}(\theta(\boldsymbol{t}), \varphi(\boldsymbol{t}))} \tag{24}$$

D. DOPPLER EFFECT ELIMITATION USING MVDR SPECTRUM ESTIMATION AND RESAMPLING METHOD

The Doppler Effect caused by the relative movement between the vehicle and the array will bring in the frequency shift and frequency band expansion of the fault characteristic frequency which will reduce the diagnosis accuracy. It can be eliminated through resampling method. The calculation of the time series for resampling is the key of this method. Among them, the center time is the most important parameter and the maximum gain can be obtained when the sound source moves into the beam pattern as shown in Fig. 2.

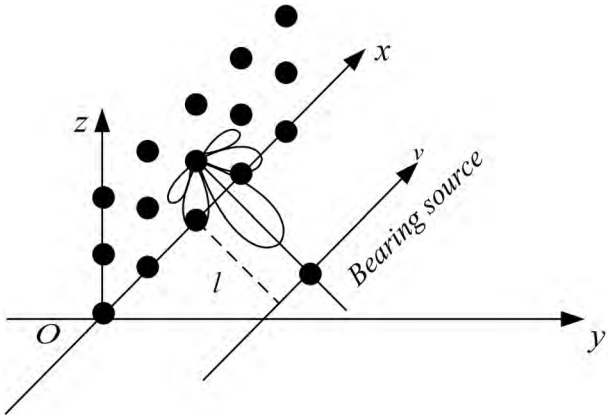

FIGURE 2. Fixed-beam filter for time center.

In this study, MVDR spectrum estimation is employed to obtain the time when the acoustic source arrives at the front of the array element at the origin point and the time series for resampling is then calculated according to the geometric parameters of the array. As shown in Fig. 3, compared with ULR, the elevation angle can be acquired due to the microphones arranged in the vertical direction. The spatial resolution of the array can be estimated much more accurately and the time series for resampling can be calculated with higher accuracy. As a result, the Doppler Effect can be eliminated more accurately. Details of the proposed Doppler Effect elimination method using MVDR spectrum estimation and resampling method is given in this section.

According to Fig. 3(b), when the acoustic source moves to the front of the array element at the origin point, the horizontal and vertical angular relative to the origin point is $\theta_{obj} = 0°$ and $\varphi_{obj} = 90°$. Substituting θ_{obj} and φ_{obj} to Eq. (10), (13) and (23), the filter weight of the OSF at this time can be calculated as:

$$\boldsymbol{w}_c = \frac{\boldsymbol{R}_{xx}^{-1}\boldsymbol{a}(\theta_c, \varphi_c)}{\boldsymbol{a}(\theta_c, \varphi_c)\boldsymbol{R}_{xx}^{-1}\boldsymbol{a}(\theta_c, \varphi_c)} \tag{25}$$

where $\boldsymbol{a}(\theta_c, \varphi_c) = [1, 1, \ldots, 1]^T$. And according to the Eq. (18), we can obtain the filtered signal as follows:

$$\boldsymbol{y}_c = \boldsymbol{w}_c^H \boldsymbol{X} \tag{26}$$

where $\boldsymbol{y}_c = [y_c(t_r(1)), y_c(t_r(2)), \ldots, y_c(t_r(\mathrm{Q}))]$. In order to calculate the time that the acoustic source arrives at the front of the array element at the origin, the instantaneous energy map (IEM) method is proposed. The basic mechanism of this method is that the peak of the energy amplitude appears when the acoustic source arrives at the front of the array element at the origin. And the corresponding energy can be calculated through the following equation:

$$E_c(t_r) = \int |rw(t_r - t) \times y_c(t)|^2 dt \tag{27}$$

And the center time can be calculated as:

$$t_c = \arg_{t_r} \max\{E_c(t_r)\} - l/c \tag{28}$$

where $rw(t_r\text{-}t)$ denotes a rectangular window with the center at t_r and the l/c expresses the time delay between the emitting time and the receiving time.

According to Eq. (28), the emitting time series of the sound source can be written as:

$$t_s(i) = [t_c - \Delta t, t_c - \Delta t + \frac{1}{2f_s}, \cdots, t_c - \Delta t + \frac{L}{2f_s}] \tag{29}$$

where $\Delta t = L/f_s$ denotes half of the time interval and $i = [1, 2, \ldots, 2L+1]$ denotes the emitting time series. Then, substituting Eq. (6) and (29) into Eq. (13) and (23), the OSF can be described as:

$$\boldsymbol{w}_{obj}(t_s) = \frac{\boldsymbol{R}_{xx}^{-1}\boldsymbol{a}(\theta(t_s), \varphi(t_s))}{\boldsymbol{a}^H(\theta(t_s), \varphi(t_s))\boldsymbol{R}_{xx}^{-1}\boldsymbol{a}(\theta(t_s), \varphi(t_s))} \tag{30}$$

$$\varphi_{m_2,i} = 90° - \frac{(m_2 - 1)dz}{\sqrt{[v(t_s(i) - t_c)]^2 + l^2 + [(m_2 - 1)dz]^2}} \times \frac{180°}{\pi} \tag{31}$$

τ'_{m1m2} can be then obtained through substituting Eq. (6) and (31) into Eq. (10), and $\boldsymbol{a}(t_s)$ can be described as:

$$\boldsymbol{a}(t_s) = [e^{-j\omega\tau'_{11}}, e^{-j\omega\tau'_{12}}, \cdots, e^{-j\omega\tau'_{m_1m_2}}, \cdots, e^{-j\omega\tau'_{M_1M_2}}] \tag{32}$$

And according to Eq. (18), the filtered signal can be calculated as:

$$\boldsymbol{y}(\boldsymbol{i}) = \boldsymbol{w}_{obj}^H(\boldsymbol{t}_s(\boldsymbol{i}))\boldsymbol{X} \tag{33}$$

The time series for resampling can be calculated by the following equation:

$$t_r(i) = t_s(i) + \frac{\sqrt{l^2 + [vt_c - vt_s(i)]^2}}{c} \tag{34}$$

Therefore, the Doppler Effect can be eliminated through resampling the filtered signal y using t_r. The resampling process is implemented by interpolating using cubic spline.

E. WHOLE SCHEME OF THE PROPOSED METHOD

The procedure of the proposed method is shown in Fig. 4, with the steps described below.

(1) Design the URA using suitable array parameters according to the characteristics of the signal.

(2) Acquire the wayside acoustic signal using the designed URA and filter the signal using bandpass filter at the interest frequency band.

(3) Obtain the filtered signal using a designed OSF based on the principle of MVDR according to Eq. (25) and calculate the time t_c using IEM method based on Eq. (27) and (28).

(4) Design an OSF based on the principle of MVDR according to Eq. (30) and filter the signal obtained in Step 2 according to Eq. (33).

(5) Calculate the time series for resampling according to Eq. (29) and eliminate the Doppler Effect through interpolation method.

(6) Diagnosis result is determined through envelope analysis of the resampled signal.

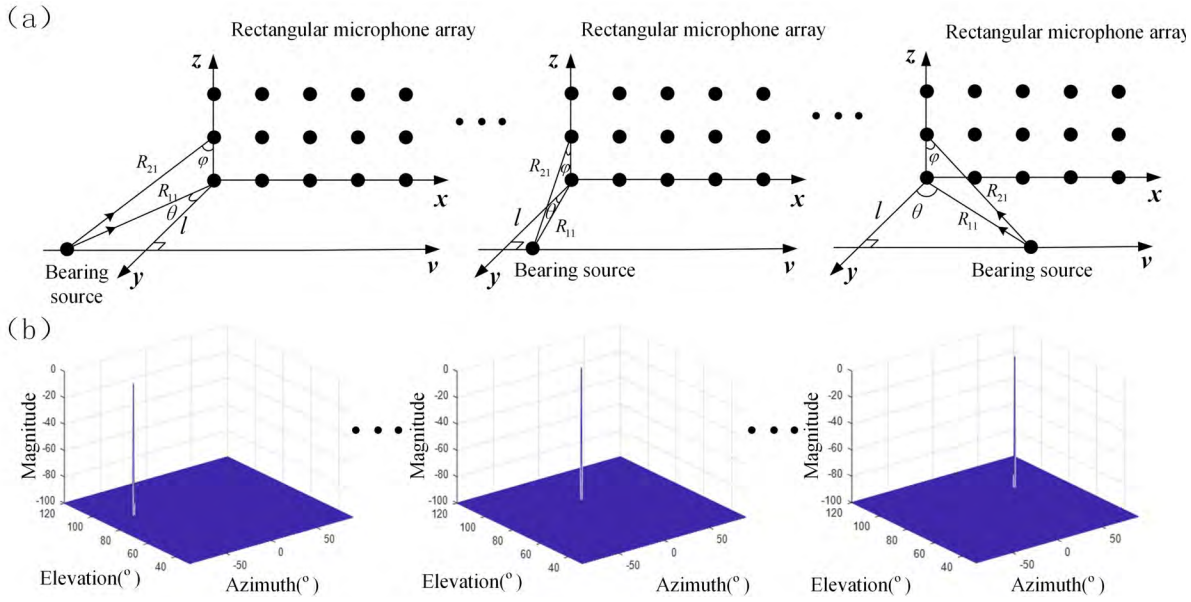

FIGURE 3. Schematic diagram of the proposed way: (a) geometric model of acoustic source motion, (b) acquire acoustic source location information using the MVDR spectrum estimation method.

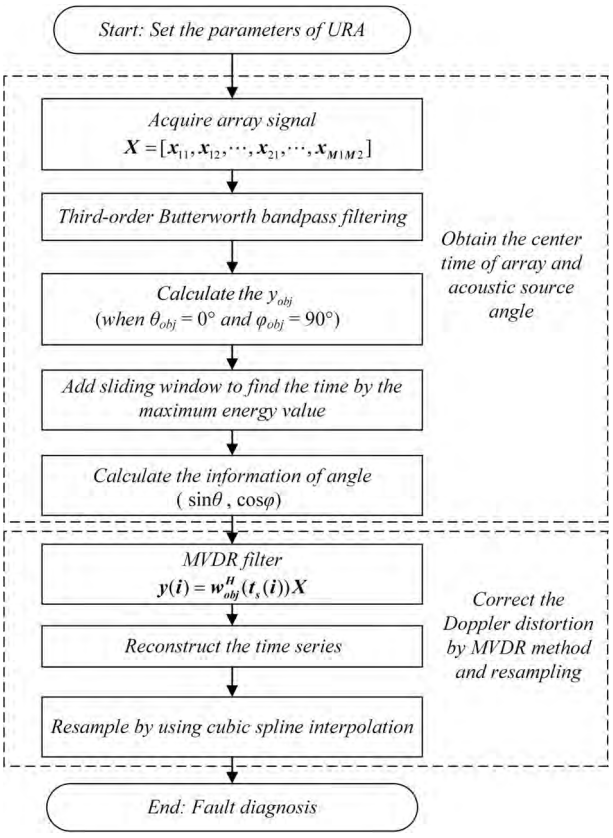

FIGURE 4. Flowchart of the proposed way in this paper.

III. SIMULATION STUDY

In this section, simulation case studies are carried out to verify the effectiveness of the proposed method. The simulated

TABLE 2. Parameters of the simulated experimental signal.

f_c Hz	A	ζ	f_p Hz	c m/s	l m	dx m	dz m	v m/s	$t_{c(1,1)}$ s
2000	1	0.03	100	340	1	0.05	0.05	50	2.0

sound source signal whelmed by noise is presented as follow:

$$q(t)=A\cos(2\pi f_c t_s)\exp[-\frac{\xi}{\sqrt{1-\xi^2}}\times 2\pi f_c \bmod (t_s,\frac{1}{f_p})]+v(t) \tag{35}$$

where $A = 1$ represents the amplitude; f_c denotes the resonance characteristic frequency; ξ is the attenuation ration and f_p reflects the fault characteristic frequency; mod (a, b) is the remainder of a divided by b, which produces periodic waveform; $v(t)$ is represents the added noise subjected to a normal Gaussian distribution. The sampling frequency is 10 kHz and the sampling point number is 40000. Other experimental parameters are shown in Table 2.

The simulated signal received by the microphone element located at (m_1, m_2) embedded with Doppler distortion can be obtained by substituting Eq. (35) into Eq. (7).

The simulated signal without noise is firstly analyzed by the two methods. That means the $v(t)$ in Eq. (35) is set to be 0. The waveform of the Doppler-shifted signal received by the microphone element located at the origin point is shown in Fig. 5(a). It can be seen that the signal has been significantly distorted by Doppler Effect in the time domain. The phenomenon of frequency shift and expansion can be seen from the frequency spectrum and envelope spectrum

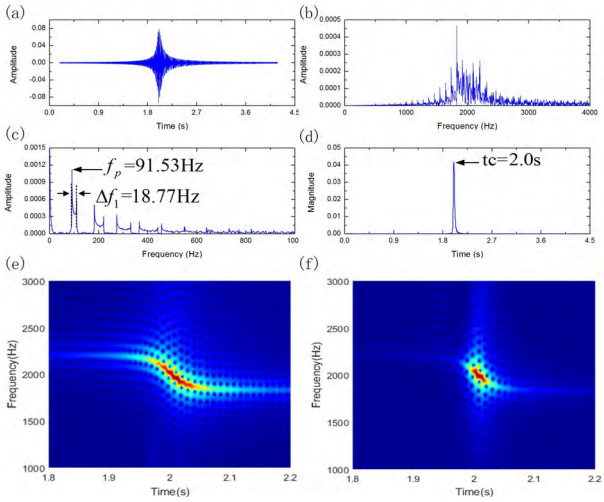

FIGURE 5. Simulated uncorrected Doppler signal with no noise: (a) waveform, (b) spectrum, (c) envelope spectrum, (d) instantaneous energy curve, (e) TFD of the distortion signal, (f) TFD of the central moment.

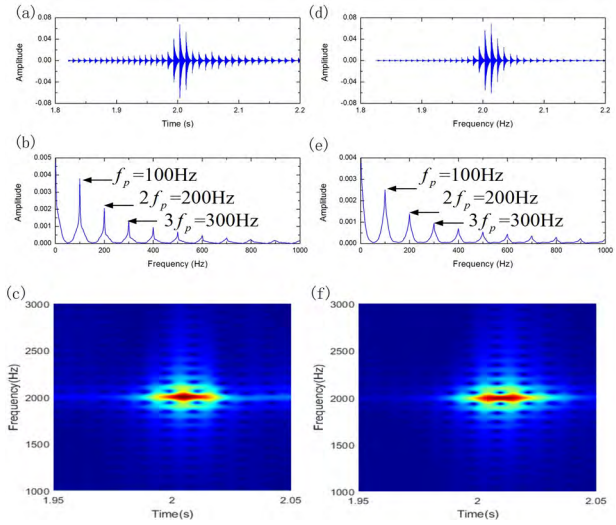

FIGURE 6. Results of the corrected Doppler signal: (a) the waveform by the ULA, (b) envelope spectrum by the ULA, (c) TFD of the corrected signal by the ULA, (d) the waveform by the proposed URA, (e) envelope spectrum by the proposed URA, (f) TFD of the corrected signal by the proposed URA.

shown in Fig. 5(b) and (c) which indicates the distortion by Doppler Effect in the frequency domain.

Firstly, the ULA method proposed by Zhang *et al.* [42] is employed to process the signal. The ULA is designed according to the model shown in Fig.1 (a) with 5 microphones arranged into a line. The parameters dx and l are set to be 0.05 m and 1 m respectively. According to the procedure presented by Zhang *et al.* [42], firstly, the signal obtained by the ULA is filtered through a low-pass filtering with cutoff frequency of 500 Hz. Secondly, the zero-angular spatial filtering algorithm is applied to calculate the central moment $t_c = 2.0$ s when the sound source reaches the front of the microphone at the origin point. Thirdly, the receiving time series t_r are calculated according to the relation between t_c, t_r and the emission time series t_s expressed by Eq. (34). Finally, the Doppler Effect is eliminated through interpolation method. The corrected signal is shown in Fig. 6(a) with its envelope spectrum and time-frequency distribution (TFD) shown in Fig. 6(b) and (c).

Then, the proposed URA method is employed to process the signal. Firstly, a URA consisting of 15 microphone elements arranged into 5 columns and 3 rows is designed. Parameters of the URA are shown in Table 1. The vertical distance l is set to be 1m to satisfy the far-field condition ($l > 0.47$ m) expressed by Eq. (9). Secondly, the signal is filtered using a 3 order Butter-worth band-pass filter at [500 Hz, 3000 Hz]. Thirdly, an OSF based on the principle of MVDR is established using Eq. (25) to filter the signal obtained in the previous step. The TFD of the filtered signal is shown in Fig. 5(f). Then the IEM method is employed to calculate the instantaneous energy according to Eq. (27) and (28) and the curve of the calculated instantaneous energy is shown in Fig. 5(d). The time value of $t_c = 2.0$ s can be determined as the time when the acoustic source arrives at the

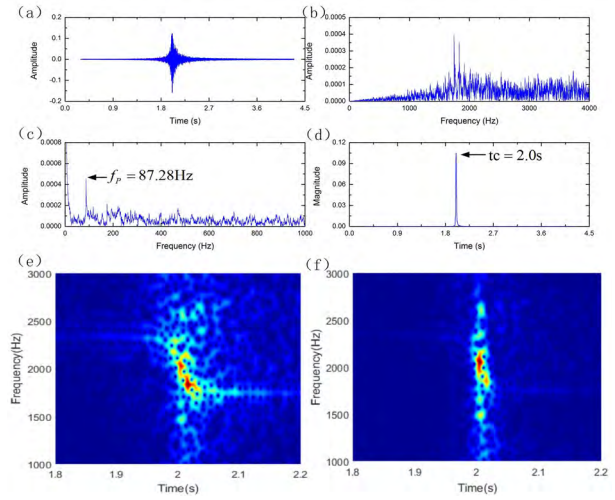

FIGURE 7. Simulated uncorrected Doppler signal with noise and SNR = −30.7dB: (a) waveform, (b) spectrum, (c) envelope spectrum, (d) instantaneous energy curve, (e) TFD of the distortion signal, (f) TFD of the central moment.

front of the array element at the origin point. Fourthly, an OSF is designed according to Eq. (30) and employed to filter the signal obtained in the second step. Then, the time series for resampling is calculated according to Eq. (34) and the Doppler Effect is eliminated using cubic spline interpolation. The waveform of the corrected signal is shown in Fig. 6(d). Finally, envelope spectrum analysis is employed to determine the diagnosis result. The envelope spectrum and TFD are shown in Fig. 6(e) and (f) respectively.

It can be seen that in this simulation study without noise interface, both of the two methods have achieved good results. The phenomenon of frequency shift and expansion caused

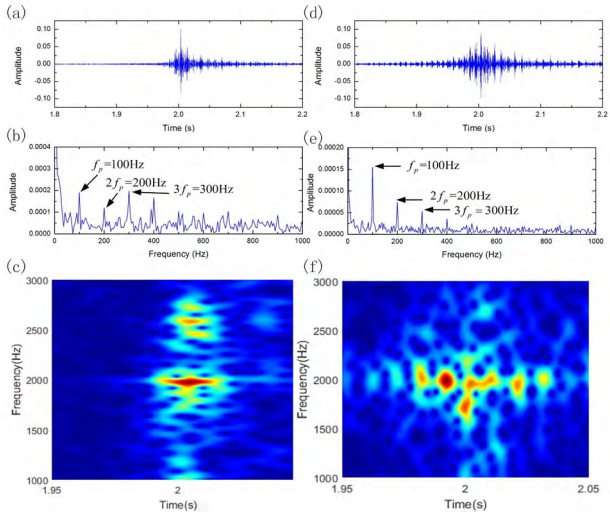

FIGURE 8. Results of the corrected Doppler signal: (a) the waveform by the ULA, (b) envelope spectrum by the ULA, (c) TFD of the corrected signal by the ULA, (d) the waveform by the proposed URA, (e) envelope spectrum by the proposed URA, (f) TFD of the corrected signal by the proposed URA.

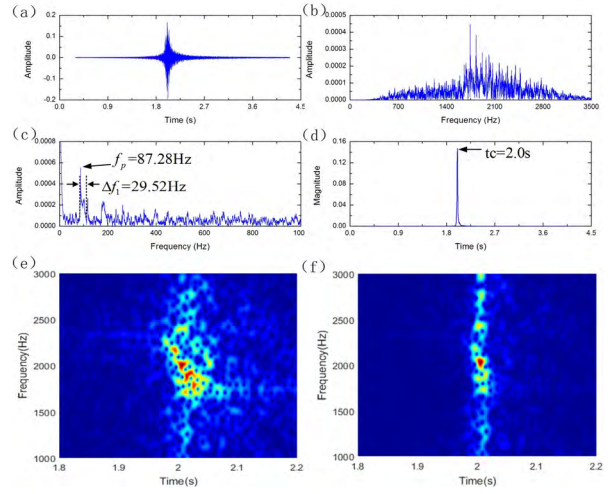

FIGURE 9. Simulated uncorrected Doppler signal with noise and SNR = −39.14dB: (a) waveform, (b) spectrum, (c) envelope spectrum, (d) instantaneous energy curve, (e) TFD of the distortion signal, (f) TFD of the central moment.

by the Doppler Effect has been eliminated and the fault characteristic frequency $f_p = 100$ Hz can be clearly found as well as the 2nd to 9th harmonics of f_p.

In order to further compare the anti-noise performance of the two methods, the SNR of the simulated signal is set to be gradually decreased and each simulated signal with different SNR is analyzed by both the two methods. When SNR becomes to be -30.7 dB, the waveform of the simulated signal is shown in Fig. 7(a) with its spectrum, envelope spectrum and TFD shown in Fig. 7(b), (c) and (e). Compared Fig. 7(c) with Fig. 5(c), it can be seen that because of the added interference of strong noise, new frequency offset has occurred. The central time calculated through the zero-angular spatial filtering

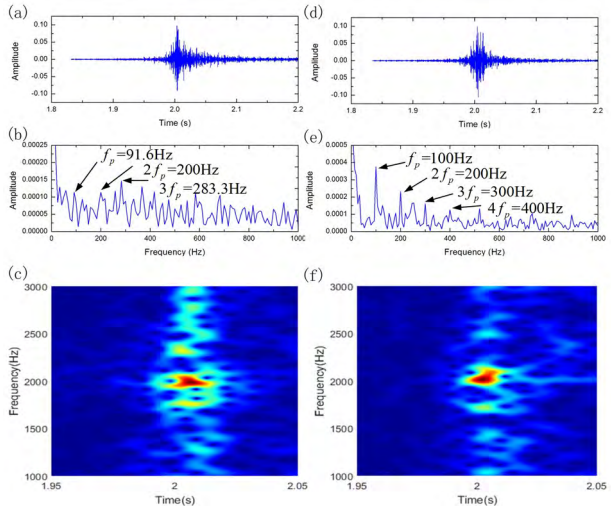

FIGURE 10. Results of the corrected Doppler signal: (a) the waveform by the ULA, (b) envelope spectrum by the ULA, (c) TFD of the corrected signal by the ULA, (d) the waveform by the proposed URA, (e) envelope spectrum by the proposed URA, (f) TFD of the corrected signal by the proposed URA.

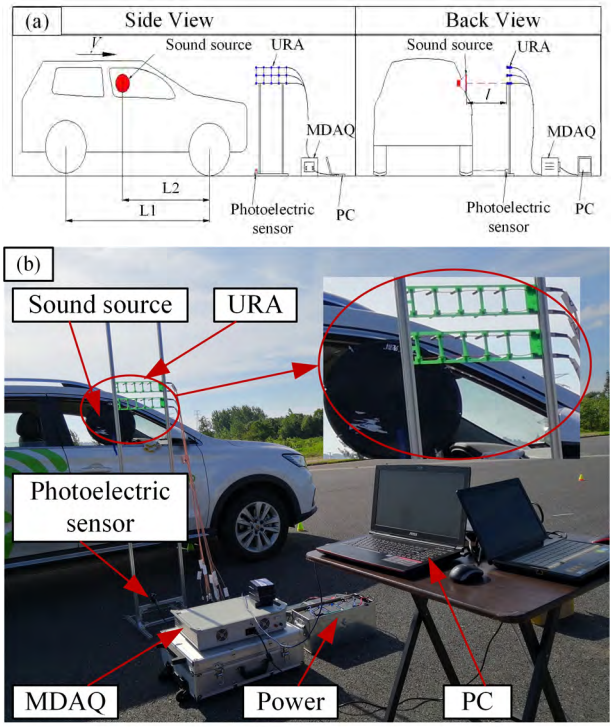

FIGURE 11. Experimental setup: (a) diagram and (b) scene.

algorithm using ULA is $t_c = 1.997$ s. From the envelope spectrum in Fig. 8(b), the phenomenon of frequency shift and expansion caused by the Doppler Effect has been eliminated and the characteristic frequency is identified as $f_p = 100$ Hz.

On the other hand, the same signal is processed by the proposed URA method. The time value of $t_c = 2.0$ s is determined through the instantaneous energy shown in Fig. 7(d)

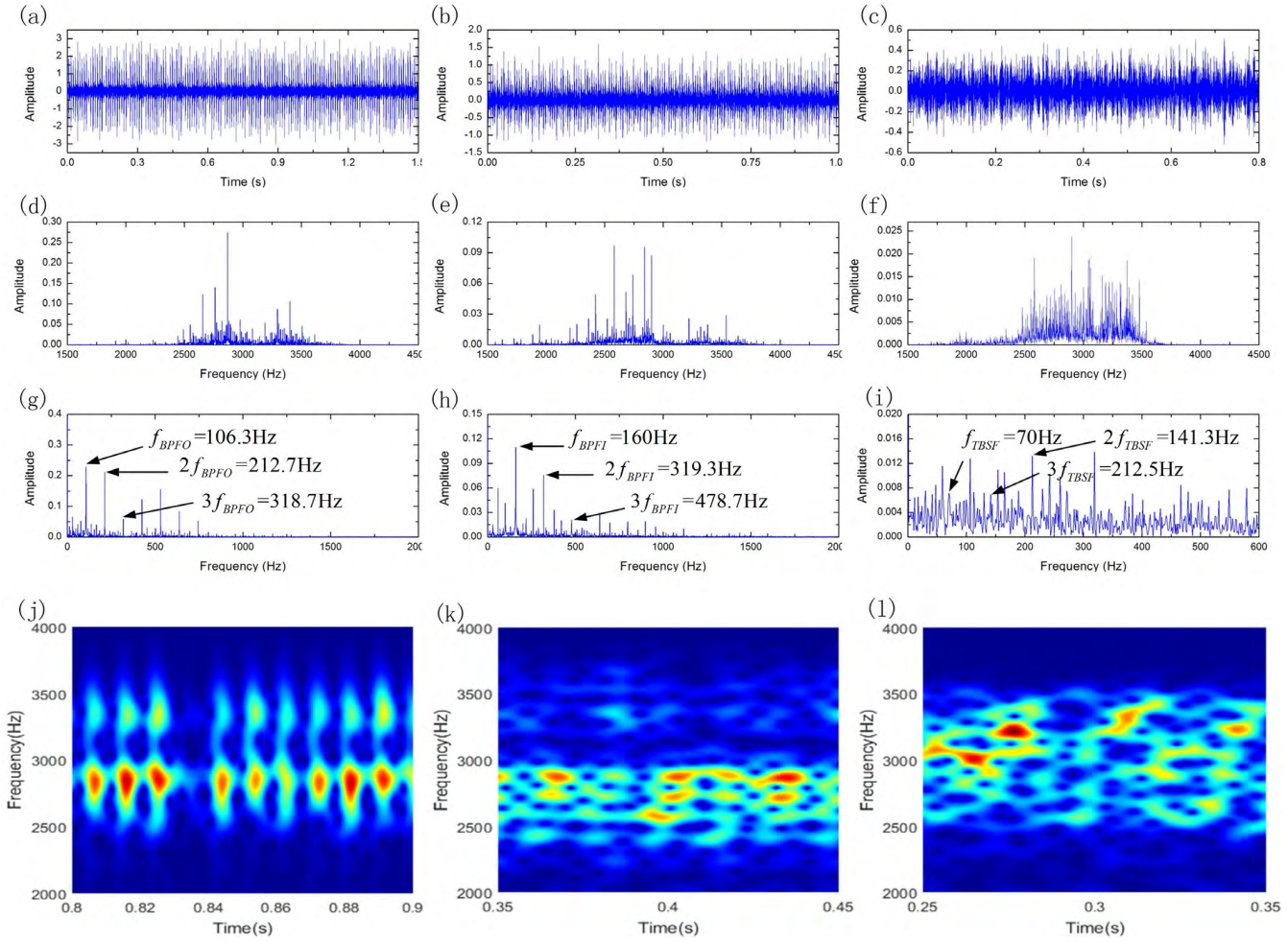

FIGURE 12. Vibration signals collected by static experiments: (a) outer-race waveform, (b) inner-race waveform, (c) roller waveform, (d) outer-race spectrum, (e) inner-race spectrum, (f) roller spectrum, (g) outer-race envelope spectrum, (h) inner-race envelope spectrum, (i) roller envelope spectrum, (j) TFD of the outer-race signal, (k) TFD of the inner-race signal, (l) TFD of the roller signal.

using the IEM method. The waveform of the corrected signal is shown in Fig. 8(d). with its envelope spectrum and TFD are shown in Fig. 8(e) and (f) respectively. It can be seen that the phenomenon of frequency shift and expansion caused by the Doppler Effect has also been eliminated and the fault characteristic frequency f_p is identified as 100 Hz which equals to the theoretical value and also the harmonics of f_p are clearly to be seen.

It can be seen that with the increase of noise intensity, both the two methods have a little error of the center time value estimation. However, the Doppler Effect can be eliminated and the characteristic frequency is identified accurately by both the two methods. When comparing the shape of the envelope spectrum shown in Fig. 8(b) with (e), it can be found that the result obtained by the proposed URA is better than ULA. In order to make a quantitative comparison, the SNR value which is defined as the ratio of the fault-relevant frequency components to fault-irrelevant frequency components is calculated. In this study, the characteristic frequency component of $f_p = 100$ Hz and the 2^{nd} to 5^{th} harmonic components are regarded as the fault-relevant frequency components and the others are regarded as the fault-irrelevant frequency components. The calculated SNRs from Fig. 8(b) and (e) are -48.35 dB and -38.28 dB respectively which indicates that the proposed URA method achieves a better signal de-noising result. The same conclusion can be reached by observing the TFD of the corrected signals shown in Fig. 8(c) and (f). The frequency components of the corrected signal by URA is much more concentrated near the resonance characteristic frequency ($f_c = 2000$ Hz).

When the SNR of the simulated signal decreased to -39.14 dB, the simulated signal with its spectrum, envelope spectrum and TFD are shown in Figs. 9(a), (b), (c) and (e) respectively. From Fig. 9(c) it can be seen that because of the further increased noise intensity and the distortion of Doppler Effect, the fault characteristic frequency shifted to 87.28 Hz and there is a frequency expansion of 29.52 Hz. The signal is firstly processed by the ULA method, the calculated central time is $t_c = 2.003$ s. From the envelope spectrum in Fig. 10(b), it can be seen that in this situation

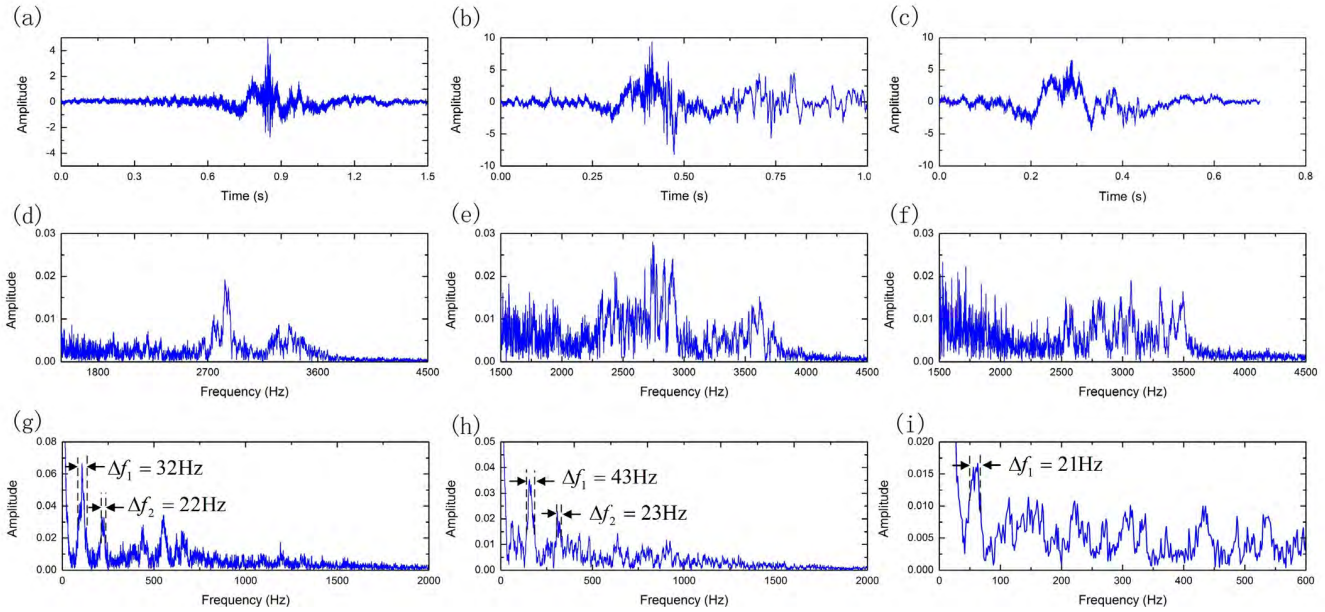

FIGURE 13. Doppler distortion signal collected by dynamic experiment: (a) outer-race waveform, (b) inner-race waveform, (c) roller waveform, (d) outer-race spectrum, (e) inner-race spectrum, (f) roller spectrum, (g) outer-race envelope spectrum, (h) inner-race envelope spectrum, (i) roller envelope spectrum.

the characteristic frequency of 100 Hz can't be identified as the domain frequency component and the closest frequency component is 91.6 Hz which has a deviation of 8.4 Hz from the theoretical value. So, in this situation, the noise intensity increased to a degree that the ULA method failed to extract the target signal. On the other hand, the central time value of $t_c = 2.0$ s is determined by the proposed URA method as shown in Fig. 9(d). The waveform of the corrected signal is shown in Fig. 10(d) with its envelope spectrum and TFD shown in Fig. 10(e) and (f) respectively. It can be seen that the characteristic frequency f_p is identified as 100 Hz which equals to the theoretical value and also the harmonic components up to the 3x can be clearly identified.

Through the simulation studies in this section, conclusions can be made that the proposed URA method performs better when the noise intensity increased due to its improved spatial directivity.

IV. EXPERIMENTAL VERIFICATION

In order to verify the superiority of the proposed method compared with ULA, three experimental case studies involving an outer-race defective bearing, an inner-race defective bearing and a roller defective bearing respectively are carried out in this section.

A. EXPERIMENT SETUP

An experiment bench including a moving vehicle with a sound source, a URA consists of 15 microphone elements arranged into 3 rows and 5 columns, a Multichannel Data Acquisition System (MDAS), a photoelectric sensor and a personal computer (PC) is designed as shown in Fig. 11 with the experimental scene in Fig. 11. The acoustic signal emitting from the sound source set on the vehicle can be collected by the array when the vehicle passes by with a certain speed. And the noise including the air dynamic noise, tire noise and the background noise will be collected simultaneously.

During the experiment, the sound source and the bottom line of the array are set on the same horizontal plane. The photoelectric sensor is set under the array to capture the time when front wheel and the back wheel of the vehicle passed by the array one after another. The captured two time points are used to locate the sound source when it comes nearest the array element at the origin point. The sound source moving speed can be calculated by the distance between the two wheels and the time delay between the two time points captured by the photoelectric sensor when the front wheel and the back wheel passes by. The bearing vibrational signal provided by the Case Western Reserve University (CWRU) is employed as the sound source signal. The bearing used in this study is the ball bearing with the type of 6205-2RS JEM SKF. The vibration data is collected with the sampling frequency of 12 kHz when the shaft was rotating at the speed of 1772 rpm. Details of the experiment can be referred to [50]. The resonance frequency band of the bearing signal in this experiment is between 2000-3300 Hz. So, to satisfy far field condition, $l > 0.47$ m, calculated by Eq. (9), the vertical distance between the sound source and the array is set to be 1m. The highest frequency of the experimental signal is 4250 Hz, so the minimum wavelength of the source is $\lambda_{\min} = 0.103$ m. To satisfy the spatial sampling theorem, the horizontal and vertical spacing between the adjacent microphone elements are both set to be 0.05 m. In the

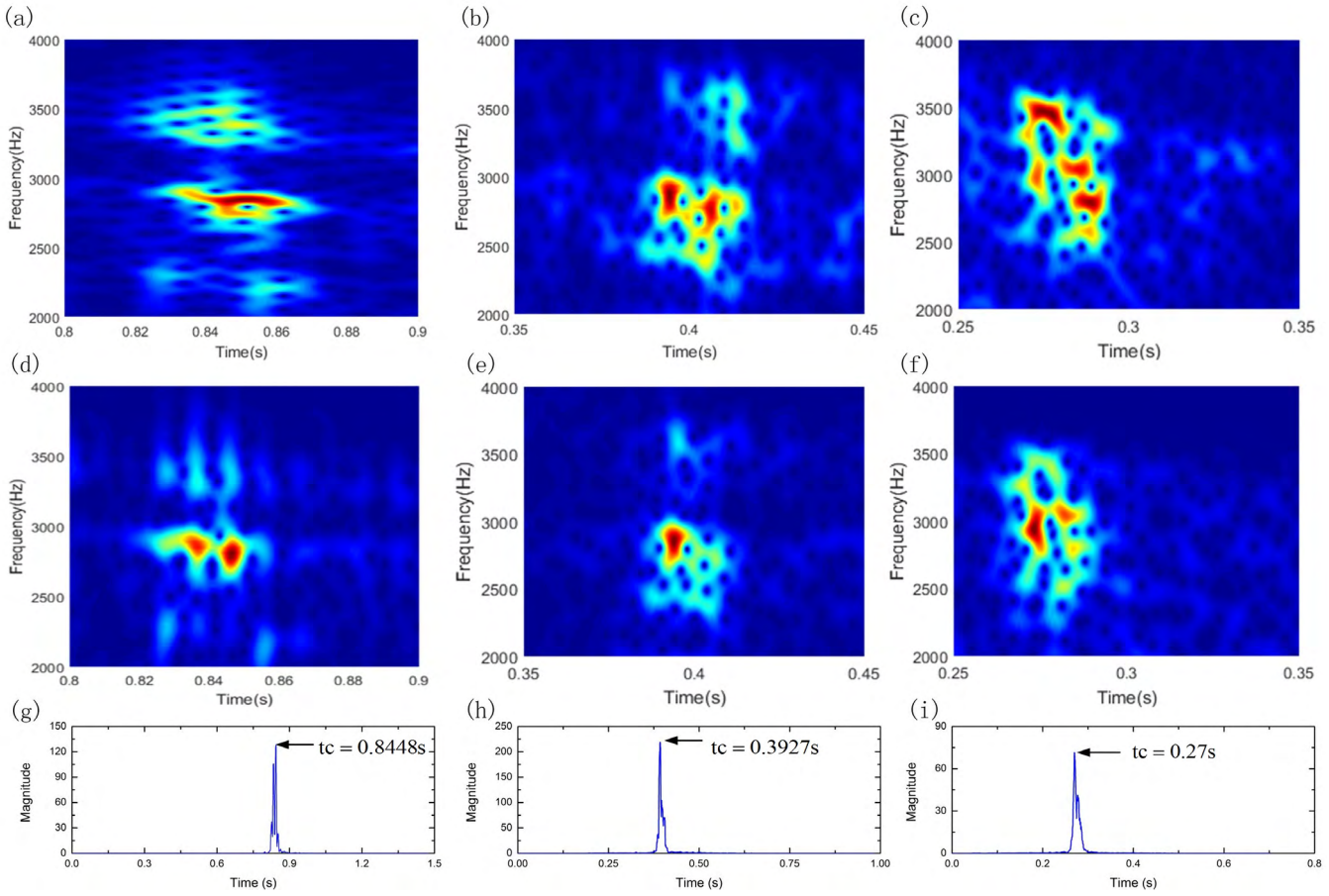

FIGURE 14. Doppler distortion signal collected by dynamic experiment: (a) TFD of the outer-race distortion signal, (b) TFD of the inner-race distortion signal, (c) TFD of the roller distortion signal, (d) TFD of the outer-race central moment, (e) TFD of the inner-race central moment, (f) TFD of the roller central moment, (g) instantaneous energy curve of the outer-race, (h) instantaneous energy curve of the inner-race, (i) instantaneous energy curve of the roller.

following, the vibration signals of three bearings with a single slit defect size of 0.007in in the outer ring, inner ring and roller respectively are used as the sound source signal. The wayside signals collected by the provided experiment bench are then analyzed by the proposed URA and traditional ULA methods and compared with each other.

In this section, three experimental wayside acoustic signals including an outer-race defective bearing signal, an inner-race defective bearing signal and a roller defective bearing signal obtained by the provided experimental bench are analyzed by the two methods. The three signals are collected under the vehicle speed of 19.26 m/s, 23.69 m/s and 26.48 m/s respectively.

The waveforms, FFT spectrums and envelope spectrums of the three experimental signals received by the microphone element located at the origin point are shown in Fig. 13. Compared with the original source bearing signals shown in Fig. 12, the distortion in both time domain and frequency domain can be clearly seen. From the envelope spectrums shown in Figs. 13(g), (h), (i), the fault characteristic frequencies are identified to be102 Hz, 154 Hz and 62.86 Hz

B. RESULTS

respectively. Compared with the theoretical values of 106.3 Hz, 159.48 Hz and 69.6 Hz, there are frequency shifts of 4.3 Hz, 5.48 Hz and 6.74 Hz respectively. What's more, there are frequency expansions of 32 Hz, 43 Hz and 21 Hz at the fault characteristic frequencies respectively which indicate that the fault-relevant energy has spread because of the Doppler Effect.

The ULA method is firstly employed to process the signals. In this study, the five microphones at the bottom of the URA shown in Fig. 10 are used as the ULA. So, according to the model shown in Fig.1 (a), the parameters dx and l are 0.05m and 1m respectively. According to the procedure presented by Zhang *et al.* [42], firstly, the signal obtained by the ULA is filtered through a band-pass filter with cutoff frequency of 2000 Hz and 4000 Hz. Secondly, the central moment when the sound source reaches the front of the microphone at the origin point is calculated using the zero-angular spatial filtering algorithm. The calculated values are $t_c = 0.8446$ s, 0.392 s and 0.2786 s respectively. Thirdly, the receiving time series t_r are calculated according to the relation between t_c, t_r and the emission time series t_s expressed by Eq. (34). Finally, the

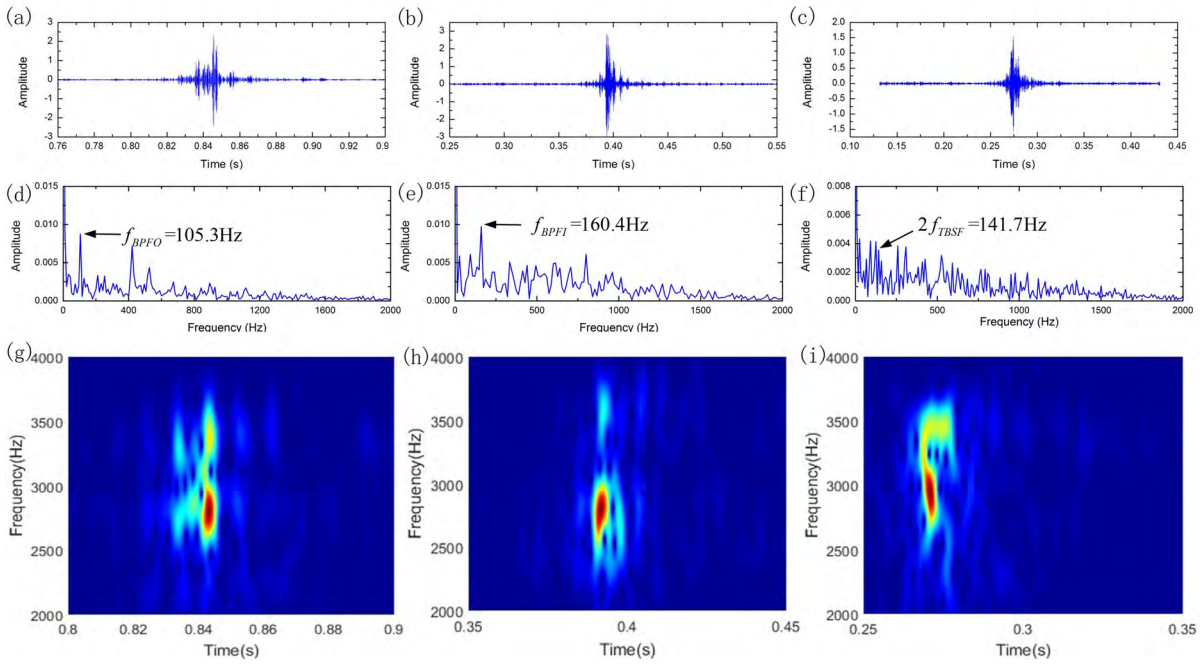

FIGURE 15. Results of Doppler distortion correction by the method of ULA: (a) waveform of the outer-race-defective bearing signal, (b) waveform of the inner-race-defective bearing signal, (c) waveform of the roller-defective bearing signal, (d) envelope spectrum of the outer-race-defective bearing signal, (e) envelope spectrum of the inner-race-defective bearing signal, (f) envelope spectrum of the roller-defective bearing signal, (g) TFD of the corrected outer-race-defective bearing signal, (h) TFD of the corrected inner-race-defective bearing signal, (i) TFD of the corrected roller-defective bearing signal.

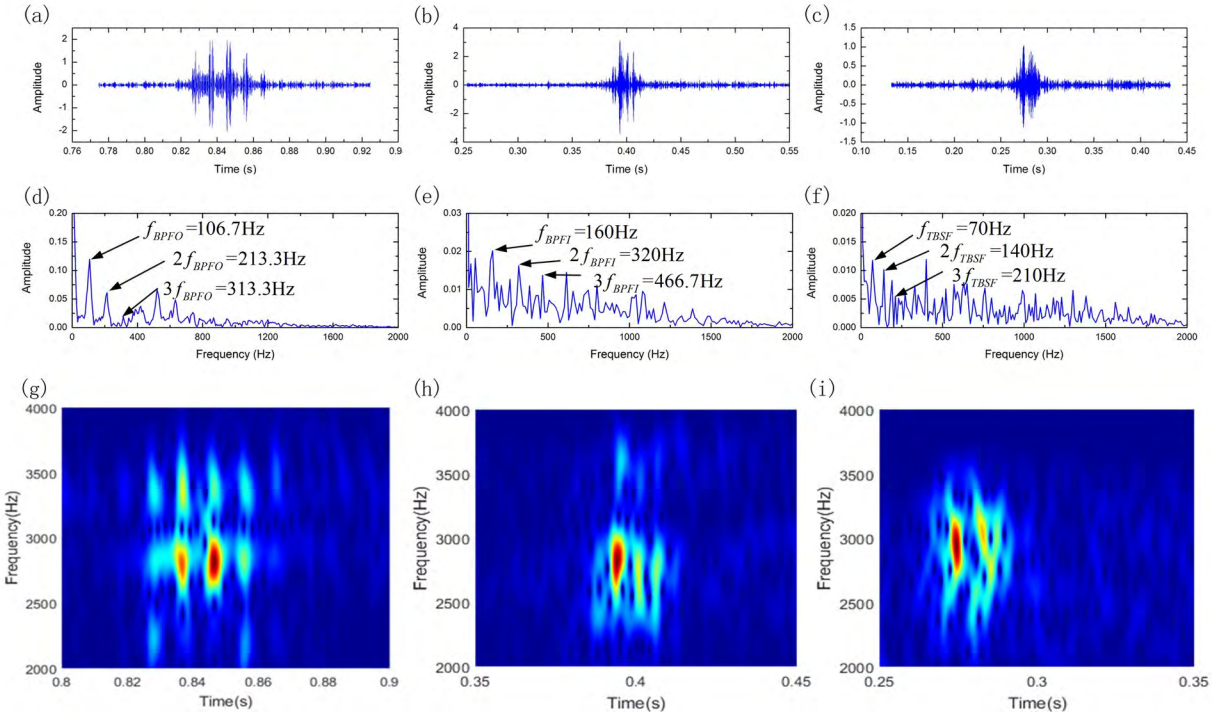

FIGURE 16. Results of Doppler distortion correction by the method of URA: (a) outer-race waveform, (b) inner-race waveform, (c) roller waveform, (d) outer-race envelope spectrum, (e) inner-race envelope spectrum, (f) roller envelope spectrum, (g) TFD of the corrected outer-race signal, (h) TFD of the corrected inner-race signal, (i) TFD of the corrected roller signal.

Doppler Effect is eliminated through resampling method. The corrected signals are shown in Figs. 15(a), (b), (c) with their envelope spectrums shown in Figs. 15(d), (e), (f) and TFDs shown in Figs. 15(g), (h), (i). The fault characteristic frequencies of 105.3 Hz, 160.4 Hz can be identified according to the envelope spectrums of the outer-race-defective bearing signal and the inner-race-defective bearing signal. The identified values have shifts of 1 Hz, 0.92 Hz respectively

TABLE 3. The identified fault characteristic frequencies from the experimental wayside signals.

Experiment	Theoretical value (Hz)	Direct analysis (Hz)	Error (Hz)	ULA (Hz)	Error (Hz)	URA (Hz)	Error (Hz)
Outer-race	106.3	102	4.3	105.3	1	106.7	0.4
Inner-race	159.48	154	5.48	160.4	0.92	160	0.52
Roller	69.6	62.86	6.74	NULL	NULL	70	0.4

from the theoretical values. However, the fault characteristic frequency of the roller-defective bearing signal, 69.6 Hz, can't be found clearly from the envelope spectrum. The peak value is identified to be 141.7 Hz which is the 2nd harmonic of the fault characteristic frequency.

Then, the proposed URA method is employed to process the signals. Firstly, all the signals captured by the array elements are filtered using a band-pass filter with cutoff frequencies of 2000 Hz and 4000 Hz. Secondly, an OSF based on the principle of MVDR is established using Eq. (25) to filter the signals obtained in the previous step. The TFDs of the three filtered signals are shown in Figs. 14(a), (b) and (c). The distortion caused by the Doppler Effect can be also seen in these TFDs compared with those of the original bearing signals shown in Figs. 12 (j), (k), (l). The IEM method is then employed to calculate the instantaneous energy according to Eq. (27) and (28). The curves of the calculated instantaneous energy are shown in Figs. 14(g), (h), (i). The time values of $t_c = 0.8448$ s, 0.3927 s and 0.27 s can be determined when the acoustic source arrives at the front of the array element at the origin point. Thirdly, an OSF is designed according to Eq. (30) and employed to filter the signals obtained in the first step. Then, the time series for resampling is calculated according to Eq. (34) and the Doppler Effect is eliminated using resampling method. The waveforms of the corrected signals are shown in Figs. 16(a), (b) and (c). Finally, envelope spectrum analysis is employed to determine the diagnosis result. The envelope spectrums and TFDs are shown in Figs. 16(d), (e), (f) and (g), (h), (i) respectively. It can be seen that the phenomenon of frequency shift and expansion caused by the Doppler Effect has been eliminated and all the fault characteristic frequencies can be clearly seen. In order to compare with the results obtained by ULA, the identified fault characteristic frequencies from the three experimental wayside signals by the two methods are listed in Table 3.

It can be seen that the errors estimated using the proposed method is much smaller than those using ULA. What's more, the ULA method failed to identify the fault characteristic frequency from the roller defective bearing signal while the proposed URA method succeed to identify it with an acceptable result with small error of 0.4 Hz. On the other hand, the 2nd and even 3rd harmonics of the fault characteristic frequency components can also be found in the envelop spectrums obtained by the proposed URA method which indicate that the much more fault-relevant signal components are extracted due to its superior spatial resolution.

V. CONCLUSIONS

To deal with the problems of strong background noise and Doppler distortion for wayside bearing fault detection, a URA consisting of 15 microphone elements combined with a designed OSF based on the principle of MVDR are introduced in this study. Results of the simulation and experimental case studies have shown that the proposed method achieved better anti-noise performance and higher diagnostic accuracy compared with traditional ULA method due to its spatial directivity improvement. The proposed method is promising to be applied in wayside acoustic bearing fault detection.

ACKNOWLEDGEMENTS

The authors would like to thank the Case Western Reserve University Bearing Data Center for providing the experiment data. The anonymous reviewers are sincerely appreciated for their valuable suggestions to improve the paper.

They would also like to thank the following senior engineers for their recommendations: Mr. Yangmin Li from the Zhengwan Passenger Railway Line Henan Company Ltd, Xinquan Li and Huigang Wan from the China Railway Zhengzhou Group Company Ltd.

REFERENCES

[1] D. Wang, K.-L. Tsui, and Q. Miao, "Prognostics and health management: A review of vibration based bearing and gear health indicators," *IEEE Access*, vol. 6, pp. 665–676, 2018.
[2] D. Wang and K.-L. Tsui, "Theoretical investigation of the upper and lower bounds of a generalized dimensionless bearing health indicator," *Mech. Syst. Signal Process.*, vol. 98, pp. 890–901, Jan. 2018.
[3] C. Li, M. Liang, Y. Zhang, and S. Hou, "Multi-scale autocorrelation via morphological wavelet slices for rolling element bearing fault diagnosis," *Mech. Syst. Signal Process.*, vol. 31, pp. 428–446, Aug. 2012.
[4] W. Huang, G. Gao, N. Li, X. Jiang, and Z. Zhu, "Time-frequency squeezing and generalized demodulation combined for variable speed bearing fault diagnosis," *IEEE Trans. Instrum. Meas.*, to be published.
[5] X. Ding and Q. He, "Energy-fluctuated multiscale feature learning with deep convnet for intelligent spindle bearing fault diagnosis," *IEEE Trans. Instrum. Meas.*, vol. 66, no. 8, pp. 1926–1935, Aug. 2017.
[6] D. Barke and W. K. Chiu, "Structural health monitoring in the railway industry: A review," *Struct. Health Monit.*, vol. 4, no. 1, pp. 81–93, Mar. 2005.
[7] M. Cerrada, R.-V. Sánchez, C. Li, F. Pacheco, D. Cabrera, J. V. de Oliveira, and R. E. Vásquez, "A review on data-driven fault severity assessment in rolling bearings," *Mech. Syst. Signal Process.*, vol. 99, pp. 169–196, Jan. 2018.
[8] Z. Tong, W. Li, B. Zhang, F. Jiang, and G. Zhou, "Online bearing fault diagnosis based on a novel multiple data streams transmission scheme," *IEEE Access*, vol. 7, pp. 66644–66654, 2019.
[9] C. Li, V. Sanchez, G. Zurita, M. C. Lozada, and D. Cabrera, "Rolling element bearing defect detection using the generalized synchrosqueezing transform guided by time–frequency ridge enhancement," *ISA Trans.*, vol. 60, pp. 274–284, Jan. 2016.
[10] C. Li, J. L. V. de Oliveira, M. Cerrada, D. Cabrera, R. V. Sánchez, and G. Zurita, "A systematic review of fuzzy formalisms for bearing fault diagnosis," *IEEE Trans. Fuzzy Syst.*, vol. 27, no. 7, pp. 1362–1382, Jul. 2018.
[11] X. P. Yan, C. H. Zhao, Z. Y. Lu, X. C. Zhou, and H. L. Xiao, "A study of information technology used in oil monitoring," *Tribol. Int.*, vol. 38, no. 10, pp. 879–886, 2005.

[12] S. L. Bepperling and A. Schöbel, *Estimation of Safety Requirements for Wayside Hot Box Detection Systems*. Berlin, Germany: Springer, 2011.
[13] B. Van Hecke, D. He, and Y. Qu, "On the use of spectral averaging of acoustic emission signals for bearing fault diagnostics," *J. Vib. Acoust.*, vol. 136, no. 6, 2014, Art. no. 061009.
[14] J. Tianxi and Q. He, "Proposal for the realization of a single-detector acoustic camera using a space-coiling anisotropic metamaterial," *Phys. Rev. Appl.*, vol. 11, Mar. 2019, Art. no. 034013.
[15] P. Zhou, S. Lu, F. Liu, Y. Liu, G. Li, and J. Zhao, "Novel synthetic index-based adaptive stochastic resonance method and its application in bearing fault diagnosis," *J. Sound Vib.*, vol. 391, pp. 194–210, Mar. 2017.
[16] Q. He, E. Wu, and Y. Pan, "Multi-scale stochastic resonance Spectrogram for fault diagnosis of rolling element bearings," *J. Sound Vib.*, vol. 420, pp. 174–184, Apr. 2018.
[17] D. Huang, J. Yang, D. Zhou, and G. Litak, "Novel adaptive search method for bearing fault frequency using stochastic resonance quantified by amplitude-domain index," *IEEE Trans. Instrum. Meas.*, to be published, 2019.
[18] R. Hao, Z. Peng, Z. Feng, and F. Chu, "Measurement science and technology application of support vector machine based on pattern spectrum entropy in fault diagnostics of rolling element bearings," *Meas. Sci. Technol.*, vol. 22, no. 4, 2011, Art. no. 045708.
[19] P.-Y. Weng and M.-K. Liu, "Roller bearing fault diagnosis based on wavelet packet decomposition and support vector machine," in *Proc. Int. Conf. Appl. Syst. Innov. (ICASI)*, May 2017, pp. 33–36.
[20] D. Wang, P. W. Tse, and Y. L. Tse, "A morphogram with the optimal selection of parameters used in morphological analysis for enhancing the ability in bearing fault diagnosis," *Meas. Sci. Technol.*, vol. 23, no. 6, pp. 65001–65015, 2012.
[21] W. Jiying and L. Zhenxing, "A self-adaptive analysis method of fault diagnosis in roller bearing based on Local mean decomposition," in *Proc. 26th Chin. Control Decision Conf. (CCDC)*, 2014, pp. 218–222.
[22] C. Shen, D. Wang, F. Kong, and P. W. Tse, "Fault diagnosis of rotating machinery based on the statistical parameters of wavelet packet paving and a generic support vector regressive classifier," *Measurement*, vol. 46, no. 4, pp. 1551–1564, May 2013.
[23] R. Yan, R. X. Gao, and X. Chen, "Wavelets for fault diagnosis of rotary machines: A review with applications," *Signal Process.*, vol. 96, pp. 1–15, Mar. 2014.
[24] H. Cui, Y. Qiao, Y. Yin, and M. Hong, "An investigation on early bearing fault diagnosis based on wavelet transform and sparse component analysis," *Struct. Health Monitor.*, vol. 16, pp. 39–49, Jan. 2017.
[25] S. Hou, Y. Li, and Z. Wang, "A resonance demodulation method based on harmonic wavelet transform for rolling bearing fault diagnosis," *Struct. Health Monitor.*, vol. 9, no. 4, pp. 297–308, Nov. 2010.
[26] D. Wang, Q. Miao, and R. Kang, "Robust health evaluation of gearbox subject to tooth failure with wavelet decomposition," *J. Sound Vib.*, vol. 324, no. 3, pp. 1141–1157, Jul. 2009.
[27] H. C. Choe, Y. Wan, and A. K. Chan, "Neural pattern identification of railroad wheel-bearing faults from audible acoustic signals: Comparison of FFT, CWT, and DWT features," *Proc. SPIE*, vol. 3078, pp. 480–496, 1997.
[28] R. L. Florom, A. R. Hiatt, J. E. Bambara, and R. L. Smith, "Wayside acoustic detection of railroad roller bearing defects," in *American Society of Mechanical Engineers Winter*, 1988.
[29] W. Xiong, Q. He, K. Ouyang, and Z. Peng, "Combining spatial filtering and sparse filtering for coaxial-moving sound source separation, enhancement and fault diagnosis," *IEEE Access*, vol. 7, pp. 25150–25162, 2019.
[30] F. D. Irani, *Development and Deployment of Advanced Wayside Condition Monitoring Systems*. Foregin Roling Stock, 2002.
[31] J. Dybała and S. Radkowski, "Reduction of Doppler effect for the needs of wayside condition monitoring system of railway vehicles," *Mech. Syst. Signal Process.*, vol. 38, no. 1, pp. 125–136, 2013.
[32] J. Wang, Q. He, and F. Kong, "A new synthetic detection technique for trackside acoustic identification of railroad roller bearing defects," *Appl. Acoust.*, vol. 85, pp. 69–81, Nov. 2014.
[33] C. Shen, G. Cai, Z. He, W. Huang, and Z. Zhu, "A parameterized Doppler distorted matching model for periodic fault identification in locomotive bearing," *Proc. Inst. Mech. Eng., C, J. Mech. Eng. Sci.*, vol. 230, no. 20, pp. 3791–3802, 2016.
[34] Q. He, J. Wang, F. Hu, and F. R. Kong, "Wayside acoustic diagnosis of defective train bearings based on signal resampling and information enhancement," *J. Sound Vib.*, vol. 332, pp. 5635–5649, Oct. 2013.
[35] C. Shen, F. Liu, D. Wang, A. Zhang, F. Kong, and P. W. Tse, "A Doppler transient model based on the laplace wavelet and spectrum correlation assessment for locomotive bearing fault diagnosis," *Sensors*, vol. 13, no. 11, pp. 15726–15746, 2013.
[36] H. Zhang, S. Zhang, Q. He, and F. Kong, "The Doppler effect based acoustic source separation for a wayside train bearing monitoring system," *J. Sound Vib.*, vol. 361, pp. 307–329, Jan. 2016.
[37] J. Wang, Q. He, and F. Kong, "Automatic fault diagnosis of rotating machines by time-scale manifold ridge analysis," *Mech. Syst. Signal Process.*, vol. 40, no. 1, pp. 237–256, Oct. 2013.
[38] S. Zhang, S. Lu, Q. He, and F. Konga, "Time-varying singular value decomposition for periodic transient identification in bearing fault diagnosis," *J. Sound Vib.*, vol. 379, pp. 213–231, Sep. 2016.
[39] F. Liu, Q. He, F. Kong, and Y. Liu, "Doppler effect reduction based on time-domain interpolation resampling for wayside acoustic defective bearing detector system," *Mech. Syst. Signal Process.*, vol. 46, no. 2, pp. 253–271, 2014.
[40] H. Fei, Q. S. Chang, L. Fang, Z. Ao, and R. K. Fan, "Doppler shift elimination method based on instantaneous frequency estimation for the wayside acoustic signal," *Appl. Mech. Mater.*, vol. 333, pp. 510–515, May 2013.
[41] F. Liu, C. Shen, Q. He, A. Zhang, F. Kong, and Y. Liu, "Doppler effect reduction scheme via acceleration-based Dopplerlet transform and resampling method for the wayside acoustic defective bearing detector system," *Proc. Inst. Mech. Eng., C, J. Mech. Eng. Sci.*, vol. 228, no. 18, pp. 3356–3373, 2014.
[42] S. Zhang, Q. He, K. Ouyang, and W. Xiong, "Multi-bearing weak defect detection for wayside acoustic diagnosis based on a time-varying spatial filtering rearrangement," *Mech. Syst. Signal Process.*, vol. 100, pp. 224–241, Feb. 2018.
[43] X. Liu, Z. Hu, Q. He, S. Zhang, J. Zhu, and X. Liu, "Doppler distortion correction based on microphone array and matching pursuit algorithm for a wayside train bearing monitoring system," *Meas. Sci. Technol.*, vol. 28, no. 10, 2017, Art. no. 105006.
[44] S. Dharanipragada and B. D. Rao, "MVDR based feature extraction for robust speech recognition," in *Proc. IEEE Int. Conf. Acoust., Speech, Signal Process.*, May 2001, pp. 309–312.
[45] S. Dharanipragada, U. H. Yapanel, and B. D. Rao, "Robust feature extraction for continuous speech recognition using the MVDR spectrum estimation method," *IEEE Trans. Audio, Speech, Language Process.*, vol. 15, no. 1, pp. 224–234, Jan. 2007.
[46] J. Chen, J. Benesty, and Y. Huang, "A minimum distortion noise reduction algorithm with multiple microphones," *IEEE Trans. Audio, Speech, Language Process.*, vol. 16, no. 3, pp. 481–493, Mar. 2008.
[47] P. M. Morse, K. U. Ingard, and F. B. Stumpf, "Theoretical acoustics," *Phys. Today*, vol. 22, pp. 98–99, 1969.
[48] P. E. Holbourn, *Phased Array Antenna Handbook*, 2nd ed. R. J. Mailloux, Ed. London, U.K.: Artech House, 2005. p. 496.
[49] D. H. Johnson and E. D. Dan. *Array Signal Processing: Concepts and Techniques*. Upper Saddle River, NJ, USA: Prentice-Hall, 1992.
[50] [Online]. Available: http://csegroups.case.edu/bearingdatacenter/pages/download-data-file

HAIDONG HUANG received the B.S. degree in automation from Chaohu University, Hefei, China, in 2017.

He is currently pursuing the M.S. degree with the College of Electric Engineering and Automation, Anhui University, Hefei. His research interest includes signal-processing-based machine fault diagnosis.

FANG LIU received the B.S. and Ph.D. degrees in mechanical engineering from the University of Science and Technology of China, Hefei, China, in 2009 and 2014, respectively.

He is currently an Associate Professor with the College of Electrical Engineering and Automation, and with the National Engineering Laboratory of Energy-Saving Motor and Control Technology, Anhui University, Hefei. His current research interests include machinery condition-based monitoring and fault diagnosis, signal processing, and robotics.

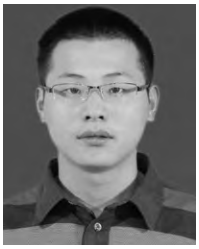

LIN GENG received the B.S. and Ph.D. degrees in mechanical engineering from the Hefei University of Technology of China, Hefei, China, in 2011 and 2016, respectively.

He is currently a Lecturer with the College of Electrical Engineering and Automation, Anhui University, Hefei. His current research interests include noise testing, analysis and control, near-field acoustic holography, and beamforming.

YONGBIN LIU received the M.S. and Ph.D. degrees in mechanical engineering from the University of Science and Technology of China, Hefei, China, in 2004 and 2011, respectively.

He is currently a Professor with the College of Electrical Engineering and Automation and with the National Engineering Laboratory of Energy-Saving Motor and Control Technology, Anhui University, Hefei. His current research interests include smart material actuators, and machinery condition monitoring and fault diagnosis.

ZIHUI REN received the Ph.D. degree in systems engineering from Tongji University, Shanghai, China, in 2011.

She is currently the Chairman of Anhui Fuhuang Technology Company Ltd. Her current research interests include intelligent transportation and railway transportation safety, smart city construction, and operation and public safety.

YUKUN ZHAO is the Executive Deputy General Manager with Anhui Fuhuang Technology Company Ltd. His current research interests include intelligent transportation and railway transportation safety.

XIUJUN LEI received the B.S. and Ph.D. degrees in mechanical engineering from the University of Science and Technology of China, Hefei, China, in 2011 and 2016, respectively.

He is currently a Lecturer with the School of Instrument Science and Electro-Optics Engineering, Hefei University of Technology, and he is also the Vice-General Manager with Hefei Fuhuang Junda High-Tech Information Technology Company Ltd. His current research interests include visual measurement and image processing.

XIAOYIN LU received the B.S. degree in electronic science and technology and the M.S. degree in biomedical engineering from the University of Science and Technology of China, Hefei, China, in 2010 and 2013, respectively. After graduation, he was a Senior Product Manager with Hefei Meyer Optoelectronic Technology Inc. He was involved in research and development of photoelectric sorting equipment. He is currently the Director of the Research and Development Department, Hefei Fuhuang Junda High-Tech Information Technology Company Ltd. His current research interests include high-speed image sensing and visual imaging.